



# Optimization analysis of NPR cable support considering bearing structure in the NSF condition of deep shaft based on Daqiang coal mine

Chengwei Zhao<sup>1,2</sup> · Xiaoming Sun<sup>1,2</sup> · Yong Zhang<sup>1,2</sup> · Shangkun Zhang<sup>1,2</sup> · Jiaxuan Zhang<sup>1,2</sup>

Received: 12 October 2020 / Accepted: 12 August 2021 / Published online: 4 September 2021  
© Saudi Society for Geosciences 2021

## Abstract

The deep soft rock shaft with non-uniform stress is a technical challenge for the selection of support parameters. In order to obtain the stress distribution, failure mode, and control characteristics of shaft surrounding rock under non-uniform stress field (NSF), a shaft model under non-uniform stress field was established by numerical simulation software of FLAC3D. The characteristics of maximum stress-bearing circle and plastic zone were investigated using theoretical analysis and numerical simulation. The maximum stress-bearing circle and plastic zone increased with the increase of the NSF coefficient. The peak stress in the  $y$ -axis direction increased, while the peak stress in the  $x$ -axis direction decreased. However, the change of the plastic zone in the  $x$ -axis was not obvious. The negative Poisson's ratio (NPR) cable was proposed to control the stability of the shaft, and the optimal support schemes with space of 1000 mm and length of 8 m were obtained by comparing the plastic zone, maximum stress-bearing circle, and shaft failure. The results indicated that the optimal support scheme reduced the plastic zone and failure significantly, which indicated that NPR cable support could effectively improve the bearing capacity of the shaft. The optimal NPR cable support scheme was also applied to control the stability of the shaft in field test. According to 200 days of monitoring data, the deformation of the surrounding rock is very small, which provides guidance for shaft support.

**Keywords** FLAC3D · Negative Poisson's ratio (NPR) cable · Non-uniform stress field (NSF) · Maximum stress-bearing circle · Plastic zone

## Introduction

The shaft is the most critical channel for mine transportation, ventilation, and various pipelines, which plays a vital role in guaranteeing coal mine's safety production. With the deep shaft developing into the deep part, there are some hazardous phenomena, including rockburst, gas explosion, large deformation, and high water pressure, making the engineering more difficult and dangerous (Walton et al. 2018; Strickland et al.

2016). These phenomena are closely associated with high stress. Due to the unique geomechanical environment, the deep rock mass presents non-linear mechanical failure characteristics. Therefore, it is significant to study the stress, failure characteristics, and stability control of deep shaft surrounding rock.

The non-uniform stress of shaft surrounding rock usually comes from the inhomogeneous lithology, structure, in situ stress, and seepage of the surrounding rock. Guo et al. (2008) emphasized that the shaft's non-uniformity led to the tensile stress in the shaft. The calculation formula of shaft wall thickness is deduced under the condition of the shaft suffering from compressive stress through the theoretical solution. Based on the Geological Strength Index (GSI), Sun et al. (2018) describes the deformation and stress characteristics of the surrounding rock and shaft liner under a soft and hard rock. The results indicated that the maximum shear stress and plastic zone appear near the interface between soft and hard rocks, which resulted in the failure of the deep shaft. The control methods of advance grouting and pressure relief

---

Responsible Editor: Murat Karakus

✉ Xiaoming Sun  
108830@cumt.edu.cn

<sup>1</sup> State Key Laboratory for Geomechanics and Deep Underground Engineering, China University of Mining and Technology (Beijing), Beijing 100083, China

<sup>2</sup> School of Mechanics and Civil Engineering, China University of Mining and Technology (Beijing), Beijing 100083, China

excavation were proposed to control the shaft's stability. Based on Mohr-Coulomb's strength theory, Xu et al. (2005) discussed the stress distribution laws and stress variation laws in a critical point in the shaft. The results provided a reference for the research of the shear force between the pile stake and soil. Akl and Whittle (2016) established a numerical model of a thick-walled cylinder test to investigate the stability of the vertical shaft in hard clays.

Based on the background of Suncun thousand meters mine, Wang (1993) calculated the shaft wall thickness of the deep shaft combining with in situ stress measurement results, which provided a reference for the wall design of the mining area. Through the analysis of the shaft force, Gough and Bell (1982) pointed out that the shaft fracture usually occurs in the direction of the minimum horizontal principal stress, resulting in the elliptical deformation of the shaft. By establishing the numerical model of the wellbore model, Li et al. (2018) analyzed the coupling effect of plastic deformation and fluid flow by developing a hydro-mechanical model for the shaft. Combined with physical simulation, numerical simulation, and theoretical analysis, Yan et al. (2018) concluded that the shaft deformation and failure were induced by the movement of strata by comparing the deformation and stress variation rules during the mining. Yao et al. (2012) emphasized that the failure of the shaft caused by the compressive deformation was induced by water head lowering in the aquifer.

In the aspect of shaft control technology, many scholars have done a lot of work. Kang et al. (2010) investigated the control technology of the soft rock shaft by the theoretical analysis, numerical simulation, and field test. The results showed that grouting and strong bolt and cable could control the deformation of soft and broken shaft. Cheng et al. (2011) had optimized the support structure and control measures for the instability of the deep shaft chamber group by analyzing the displacement and plastic zone in the process of excavation. Considering the technical problems in the design of deep bedrock freezing shaft support structure in the western region, Yao et al. (2010) put forward the optimization measures of shaft wall structure, such as early grouting technology for inner and outer walls and deep hole grouting for surrounding rock behind the wall. Ge (2002) adopted the elastic mechanics model and finite element numerical calculation method to verify the control technology of the ground grouting method. The result showed that the control technology could effectively prevent the fracture of the shaft wall.

Many scholars have investigated the failure mechanism and control technology of the shaft surrounding rock focused on the shallow rock stratum. However, traditional small deformation materials cannot control the deformation of the surrounding rock. Therefore, it is necessary to explore the new support technology for the stability of deep shaft. He et al.

(2014a, 2014b, 2015, 2016) invented a constant resistance bolt/cable (NPR bolt/cable) with negative Poisson's ratio effect, which was widely applied in the actual engineering of soft rock support in coal mine. Sun et al. (2014) tested the mechanical properties of NPR cable by the laboratory tensile test and field test. The results indicated that the NPR cable could effectively control the large non-linear deformation with high support resistance, large tensile capacity, and absorption capacity. Based on the method of theoretical analysis, numerical analysis, and laboratory test, Zhang et al. (2019) studied the anti-impact effect of the coupling support technology of NPR bolt/cable. Based on the NPR bolt/cable, Yang et al. (2014) adopted the coupling support scheme to support the stone gate. The results showed that the support scheme could effectively control the deformation of the stone gate.

Under the non-uniform stress field, few people have studied the distribution characteristics of stress and plastic zone of shaft surrounding rock and the stability support characteristics with NPR anchor cable in detail. First, based on the background of the auxiliary shaft of Daqiang coal mine, the plane strain elastic-plastic theory was preliminarily adopted to analyze the stress and plastic zone of the surrounding rock of the shaft. The influence factors of the maximum bearing stress circle and plastic zone have been analyzed based on the elastic-plastic theory. Then, a numerical model of shaft was established by the software FLAC3D. The evolution characteristics of the maximum stress-bearing circle and plastic zone of the shaft under the NSF were analyzed. Based on the NPR cable, the support scheme was optimized from the cable spacing and cable length. Third, the optimization scheme has been well verified in numerical simulation and field application.

## Study site

Da Qiang Coal Mine, located at the junction of Zhangqiang Town and Kangping County in Liaoning Province, is the deepest soft rock mine from the Mesozoic in China. The auxiliary shaft, the important passageway connecting ground and underground space, is the circular section with a diameter of 6 m. The design depth of the auxiliary shaft is 1000 m. The auxiliary shaft passed through many strata, and its lithology is mainly composed of coarse sandstone, siltstone, and sandy mudstone. The detailed strata histogram is illustrated in Fig. 1.

In Daqiang coal mine, the support forms of the auxiliary shaft near the ingate included NPR cable, flexible support, and shotcrete. The shape of the shaft section was circular. The radius of the shaft section was 3560 mm under no support. After support, the radius was 2750 mm. The support design of shaft section on site is shown in the Fig. 2.

Column	Geologic description	Lithology	Burial depth (m)	Thickness (m)	Horizontal elevation (m)
	Grayish white, white, better cementation	Coarse Sandstone	880.6	80	-771.1
	Grayish brown, sandy cemented, broken when meeting water	Sandy mudstone	920.6	40	-811.1
	Grayish white, white, argillaceous cement, better cementation	Siltstone	924.6	4	-815.1
	Grayish brown, sandy cemented, broken when meeting water	Sandy Mudstone	936.6	12	-827.1
	Bluish black, argillaceous cementation and broken when meeting with water	Mudstone	1010.0	73.4	-900.5

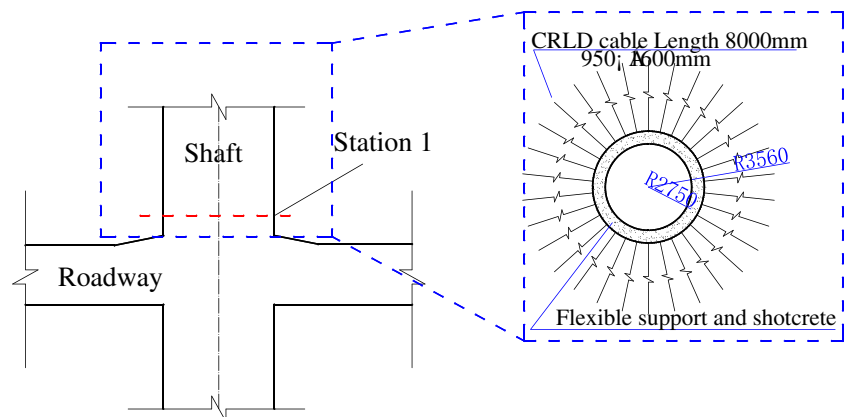
Fig. 1 Histogram of the surrounding rock

## Methodology

### Stress state and failure zone after shaft excavation

Figure 3 shows the plane strain model of the shaft. The surrounding rock is under original rock stress before the excavation of shaft. After excavation of shaft, three-dimensional stress state of deep surrounding rock changes to the state of two-dimensional stress. The stress redistribution will occur suddenly.  $\sigma_\theta$  is the tangential stress;  $\sigma_r$  is the radial stress;  $\sigma_i$  is the original rock stress. When the stress is applied to surrounding rock exceeding the bearing capacity of the rock mass, the surrounding rock will enter the plastic state. The

Fig. 2 Support scheme of shaft and monitoring station



stress-strain simplified three lines curve model of rock is adopted in this paper, as shown in Fig. 3 b. The state of the surrounding rock under stress disturbance can be divided into broken zone, plastic softening zone, and elastic zone. After the shaft excavation, the tangential stress  $\sigma_\theta$  of the surrounding rock increases. At the junction of the plastic zone and elastic zone, the tangential stress  $\sigma_\theta$  reaches the maximum value. As the stress continues to extend to the deep surrounding rock, the tangential stress  $\sigma_\theta$  returns to the original rock stress state. The circle formed by the maximum tangential stress is called the maximum stress-bearing circle. The maximum stress-bearing circle is located at the junction of the plastic zone and elastic zone. The changes of its location and value directly reflect the failure state and bearing capacity of the surrounding rock after excavation. It plays an essential role in the stability of the surrounding rock in the shaft.

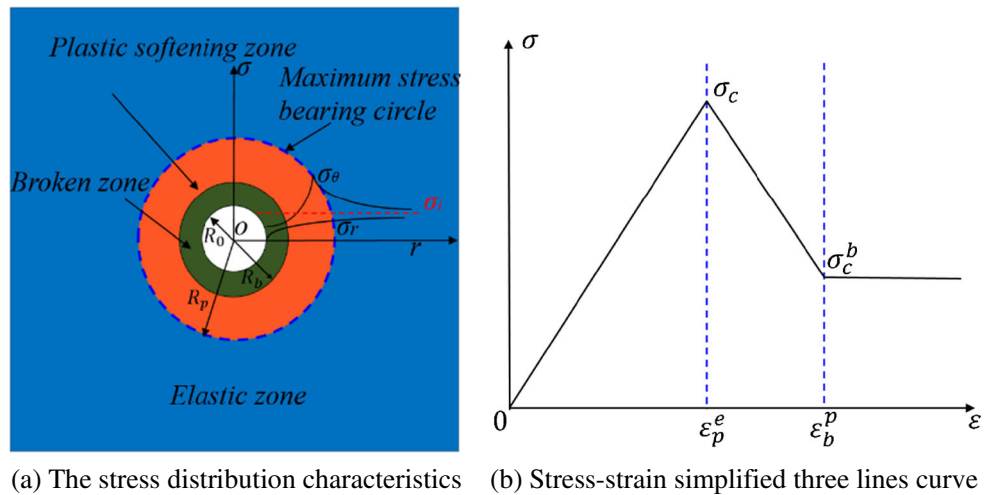
### Elastic-plastic model

In the research process, it is assumed that the rock mass is continuous, completely elastic, homogeneous, and slightly deformed, and the shaft model is an infinitely thick cylinder without considering the effect of gravity. That is to say, all the assumptions of the classical elastic theory are satisfied. The assumption of plane strain can be adopted when the influence of driving is not considered. After the excavation of the shaft, the shallow surrounding rock of the shaft is usually in the state of plastic and failure deformation. Other areas are still in an elastic state. We simplify the deformation and failure of the surrounding rock after excavating the shaft into the mechanical model shown in Fig. 4 a. Figure 4 a can be equivalent to two stress environments: the mechanical model of uniform compression shown in Fig. 4 b and the mechanical model of tension shown in Fig. 4 c.

### The elastic zone solution

According to the Fig. 4,  $R_0$  is the radius of the shaft,  $P_1 = \frac{(1+\lambda)\sigma_v}{2}$ ,  $P_2 = \frac{(1-\lambda)\sigma_v}{2}$ , and  $\lambda$  is the horizontal non-

**Fig. 3** The failure zone and stress distribution of surrounding rock. **a** The stress distribution characteristics. **b** Stress-strain simplified three lines curve



uniformity coefficient. The radial and tangential stresses in elastic zone obtained from the lame solution (Pan et al. 2015) are:

$$\sigma_r = \sigma_R \frac{R_p^2}{r^2} + P_1 \left( 1 - \frac{R_p^2}{r^2} \right) + P_2 \cos 2\theta \left( 1 - \frac{R_p^2}{r^2} \right) \left( 1 - 3 \frac{R_p^2}{r^2} \right) \quad (1)$$

$$\sigma_\theta = -\sigma_R \frac{R_p^2}{r^2} + P_1 \left( 1 + \frac{R_p^2}{r^2} \right) - P_2 \cos 2\theta \left( 1 + 3 \frac{R_p^4}{r^4} \right) \quad (2)$$

where  $\sigma_R$  is the radial stress at the interface between the plastic zone and the elastic zone of the surrounding rock of the shaft, pa;  $R_p$  is the radius of the plastic zone of the surrounding rock of the shaft, m.

**Plastic softening zone and broken zone solution**

At present, the calculation of the stress, deformation, and range in the plastic zone of underground engineering is still based on the basic point of view of the elastic-plastic theory. That is, the stress, deformation, and displacement are considered to be continuous.

Combined equilibrium differential equation with stress continuity condition, the radial and tangential stresses in the plastic softening zone are as follows:

$$\sigma_r = \frac{\sigma_c + HD}{1-\omega} + \frac{HD}{n+\omega} \left( \frac{R_p}{r} \right)^{n+1} + \left( \frac{R_p}{r} \right)^{1-\omega} \left( \sigma_R - \frac{\sigma_c + HD}{1-\omega} - \frac{HD}{n+\omega} \right) \quad (3)$$

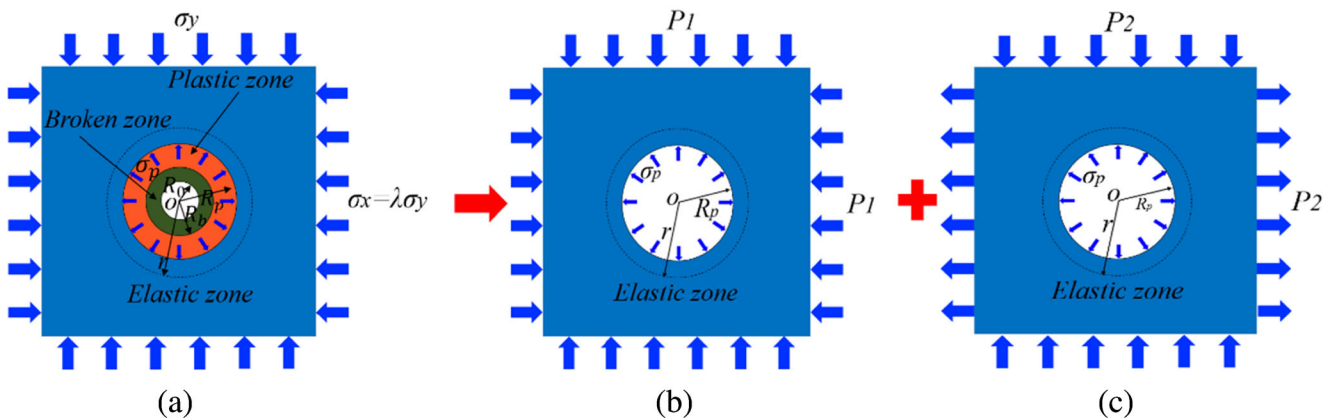


**Fig. 4** The plane strain elastoplastic model of surrounding rock of shaft: **a** non-uniform stress field model, **b** uniform compression model, **c** uniform tension and compression model

$$\begin{aligned} \sigma_\theta = & \omega \frac{\sigma_c + HD}{1-\omega} + \frac{\omega HD}{n + \omega} \left(\frac{R_p}{r}\right)^{n+1} \\ & + \omega \left(\frac{R_p}{r}\right)^{1-\omega} \left(\sigma_R - \frac{\sigma_c + HD}{1-\omega} - \frac{HD}{n + \omega}\right) \\ & + \sigma_c - HD \left[\left(\frac{R_p}{r}\right)^{n+1} - 1\right] \end{aligned} \tag{4}$$

where  $W = \frac{1+\sin\varphi}{1-\sin\varphi}$ ,  $D$  is the strength softening modulus of rock mass, and  $n$  is the expansion of plastic zone;  $H = \frac{1+\mu}{E} [2P_1(1-\mu) - \sigma_R - 4P_2(1-\mu)\cos 2\theta]$ ;  $\sigma_c^p$  is the compressive strength of rock mass in plastic softening stage.

From the stress-strain softening curve, we can get:

$$\frac{R_p}{R_b} = \left(\frac{\sigma_c - \sigma_c^b}{HD} + 1\right)^{\frac{1}{n+1}} \tag{5}$$

The radius of the broken zone  $R_b$  can be obtained from the fact that the stress on the interface of the plastic softening zone and the broken zone is continuous and the radial stress is equal:

$$R_b = R_o \left[ \frac{M}{N} + \frac{M(1-\omega)}{N(n+\omega)} + \frac{(1-\omega)}{N} \left(\sigma_R - \frac{\sigma_c + HD}{1-\omega} - \frac{HD}{n+\omega}\right) \left(\frac{M}{HD}\right)^{\frac{1-\omega}{1+n}} \right]^{\frac{1}{\omega-1}} \tag{6}$$

The radius of the plastic zone  $R_p$  and maximum stress-bearing circle:

$$R_p = R_o \left(\frac{M}{HD}\right)^{\frac{1}{1+n}} \left[ \frac{M}{N} + \frac{M(1-\omega)}{N(n+\omega)} + \frac{(1-\omega)}{N} \left(\sigma_R - \frac{\sigma_c + HD}{1-\omega} - \frac{HD}{n+\omega}\right) \left(\frac{M}{HD}\right)^{\frac{1-\omega}{1+n}} \right]^{\frac{1}{\omega-1}} \tag{7}$$

where  $M = \sigma_c - \sigma_c^b + HD$ , and  $N = P_i(1-\omega) - \sigma_c^b$ .

### Modeling approach

Through in situ stress test, it was found that the stress field of the deep surrounding rock is not uniform. The maximum principal stress of original rock stress field is horizontal stress, and the maximum horizontal stress is 34.87~39.38MPa. The maximum horizontal stress is greater than the vertical stress, and the maximum horizontal principal stress is 1.41~1.59 times of the vertical stress. The maximum horizontal principal stress is 1.25~2.10 times the minimum horizontal principal stress. The maximum principal stress, minimum principal stress, and vertical stress will form NSF environment. In this study, different lateral pressure coefficients  $\lambda$  ( $\lambda = \sigma_x/\sigma_y$ ) were considered in this paper to simulate the characteristics of NSF in the deep shaft.  $\lambda=1, 1.1, 1.2, 1.3, 1.4$ , and 2 were conducted to simulate NSF coefficients. To obtain the stress and failure

characteristics of the surrounding rock of the shaft under the NSF environment, the geometric model of shaft is established with background of Daqiang Coal Mine, as shown in Fig. 5. The model size is 50 m long, 50 m wide, and 100 m high. The shaft diameter is 6 m, and the simulation depth ranges from 900 to 1000 m. To obtain the initial stress environment of the deep shaft, the left, right, front, and rear boundaries of the model are constrained by normal displacement, and the bottom surface is constrained by fixed displacement. 22.5 MPa was applied to the model at the top to simulate the gravity stress of the upper stratum. The mechanical parameters of the surrounding rock are shown in Table 1.

The control mechanism of the high pre-stressed force of the NPR cable is shown in Fig. 6. After excavation of the shaft, the three-dimensional stress of the shallow surrounding rock is transformed into a two-dimensional stress state, as shown points A and point B in Fig. 6 b. The deep surrounding rock is still in a three-dimensional stress state, as shown point C in Fig. 6 b. When the high pre-stress is applied, the minimum principal stress of the shallow surrounding rock is increased, so points A and B begin to return to the three-dimensional stress state. The reason why NPR cable could be applied high pre-stressed force is mainly because of its constant resistance characteristics and large deformation characteristics. It can produce continuous deformation and perform excellent extension while maintaining constant resistance value. What’s more, it will show excellent resistance and energy absorption performance for high-stress dynamic load impact.

Figure 7 a shows the support principle of NPR cable. The tail of constant resistance cable is fixed with the deep surrounding rock by anchoring agent, and the end is fixed by tray and lock. The support function of constant resistance cable is divided into two stages. First stage: when the force acting on the NPR cable does not reach the constant resistance value, the constant resistance cone does not slide, as shown in Fig. 7 a; second stage: when the force acting on the NPR cable reaches the constant resistance value, the constant resistance cone slides in constant resistance sleeve with a constant resistance force.

### Optimization of NPR cable support scheme

Cable support is an effective support method in deep high-stress chambers, and the support parameters of cable often affect the support effect of the surrounding rock. In this paper, the NPR cable is applied to control the stability of deep shaft surrounding rock. In this optimization process, the NSF coefficient of 1.4 is selected to analyze the stress distribution and plastic zone of the surrounding rock. First, the optimal support spacing of NPR cable was obtained from the comparative analysis of 500mm, 1000m, 1500mm, and 2000mm; second, the optimal length is selected from 3m, 5m, 8m, and 11m under the optimal support spacing. Finally, the optimal

**Table 1** The mechanical parameters of the surrounding rock

Mechanical parameters	Density (kg/m <sup>3</sup> )	Elastic modulus (GPa)	Poisson's ratio	Cohesion (MPa)	Friction (°)
Value	2500	1.8	0.25	3	30

support spacing and length of NPR cable are selected to apply to control the stability of the shaft under NSF in numerical simulation and field test. The optimization process of NPR cable support is shown in Fig. 8.

## Results

### The analysis of theoretical solution

Based on Formulas (6) and (7), Fig. 9 shows the plastic zone ratio ( $R_p/R_0$ , the plastic zone radius to shaft radius) and the broken zone ratio ( $R_b/R_0$ , the broken zone radius to shaft radius) under different lateral pressure coefficients. As the lateral pressure coefficient increased, the plastic zone ratio and broken zone ratio increased gradually. The stress-bearing structure was far from the shaft. It indicated that the shallow surrounding rock suffers severe damage under the high NSF coefficient, and the deep surrounding rock plays a critical bearing role. As the support resistance increased, the plastic zone ratio and broken zone ratio reduced, and the stress-bearing structure was close to the shaft. It illustrated that support resistance reduced the plastic zone and broken zone, and improved the strength of the shallow surrounding rock.

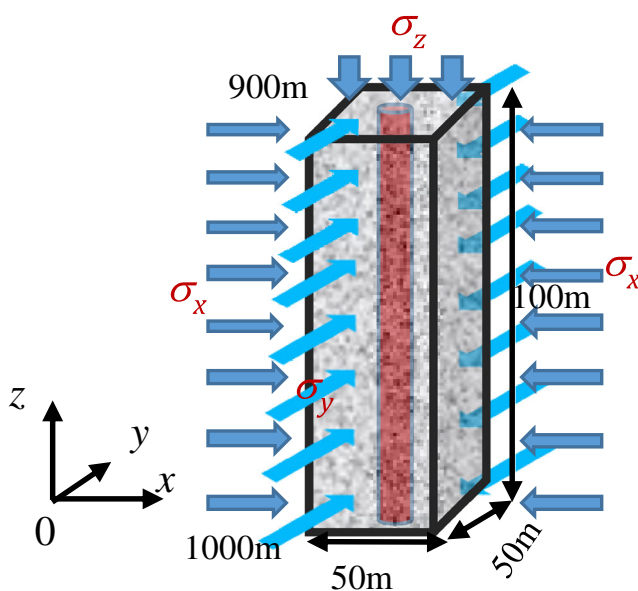


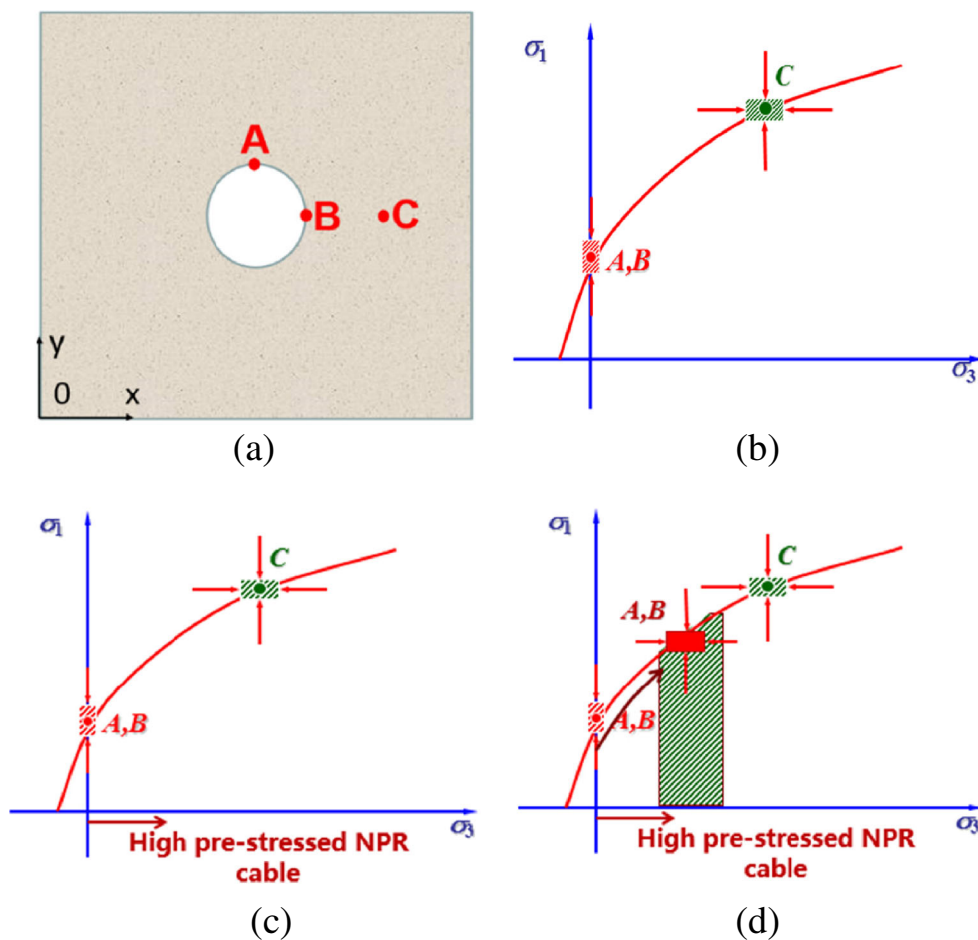
**Fig. 5** Shaft model

### Stress distribution under no support

Figure 10 shows the distribution characteristics of the maximum stress-bearing circle with a buried depth of 1000 m under no support. After the shaft excavation, the maximum stress-bearing circle was formed by the peak stress around the shaft. The stress applied in the X-axis direction is transferred and superimposed to the Y-axis direction to form the stress concentration area in the Y-axis direction, especially when the NSF coefficient is greater than 1. When the NSF coefficient was 1, the maximum stress-bearing circle presented the circular uniform distribution characteristics. As the NSF coefficient increased, the maximum stress-bearing circle began to show the elliptical shape characteristic with the long axis in the y-axis direction. The maximum stress-bearing circle's maximum value is distributed in the y-axis direction, and the minimum value of the stress-bearing circle is distributed in the x-axis direction. As the NSF coefficient increased, the stress in the y-axis direction increased, while the stress in the x-axis direction decreased, as shown in Fig. 10.

Figure 11(a, c) shows the distribution curves of the stress in the y-axis direction and in the x-axis direction, respectively. The stress curve of the surrounding rock could be generally divided into two stages: the stress growth stage and the stress-reducing and slowing down stage. After excavating the surrounding rock of the shaft, the near-field surrounding rock was in the area of the plastic zone and broken zone. The stress increased sharply to the deep surrounding rock and reached the peak stress, which was the stage of stress growth. Then, the stress decreased to the depth of the surrounding rock and tended to the original rock stress, which was the stage of stress-reducing and slowing-down stage. Figure 11(b, d) shows the Y-axis peak stress radius ratio  $R_{y,0}$  (the ratio of peak stress radius  $R_{peak}$  to shaft radius  $R_0$  in the y-axis direction) and X-axis peak stress radius ratio  $R_{x,0}$  (the ratio of peak stress radius  $R_{peak}$  to shaft radius  $R_0$  in the x-axis direction). As the NSF coefficient increased, the peak stress in the y-axis direction increased from 32 to 58 MPa, and the radius ratio  $R_{y,0}$  increased from 3.73 to 6.3 (Fig. 11(b)). The peak stress in the x-axis direction decreased from 32 to 22 MPa, and the radius ratio  $R_{x,0}$  increased from 3.73 to 4.25 (Fig. 11(d)). It should be noted that the

**Fig. 6** The mechanical transformation mechanism of high pre-stressed NPR cable support: **a** excavation model of shaft; **b** stress analysis of points A, B, and C; **c** application of high pre-stress in NPR cable; **d** improvement of the stress state of points A and B



change of peak stress radius in the  $x$ -axis direction was not obvious when the NSF coefficient increased from 1 to 2.

**Plastic zone distribution under no support**

The plastic zone indicates the failure degree of the surrounding rock, which plays a vital role in the support design and the selection of support parameters. Figure 12 shows the expansion range of the plastic zone. According to the distribution characteristics of the plastic zone, when the NSF coefficient is 1, the plastic zone of the shaft surrounding rock presented the uniform circular distribution characteristics. When the NSF coefficient is greater than 1, the plastic zone showed the elliptical shape with the long axis in the  $y$ -axis direction. The larger the NSF coefficient is, the more obvious the elliptical effect of the plastic zone. It should be noted that the changes of the plastic zone radius in the  $x$ -axis direction were not obvious with the increase of the NSF coefficient, which is stable between 10 and 11m. The plastic zone radius of the  $y$ -axis increased from 10.56 to 19.4 m when the NSF coefficient varied from 1 to 2, an increment of 83.7% (Fig. 12(g)). It is worth noting that when the lateral pressure coefficient is 2, the plastic zone of the surrounding rock presents a butterfly shape.

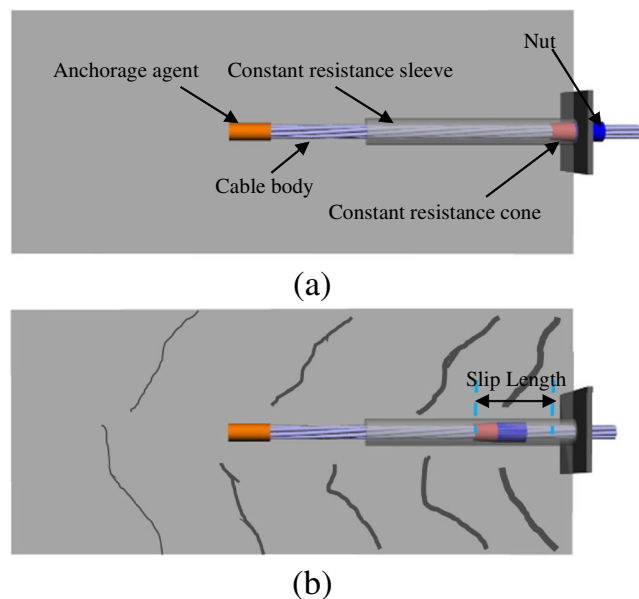


**Fig. 7** The support principle of NPR cable: **a** interaction between NPR cable and surrounding rock; **b** NPR cable sliding with constant resistance

Figure 13 shows the failure characteristics of the plastic zone under no support. We define the shear failure (shear failure is defined as  $D_s = \frac{V_s}{V} \times 100\%$  where  $V_s$  is the total

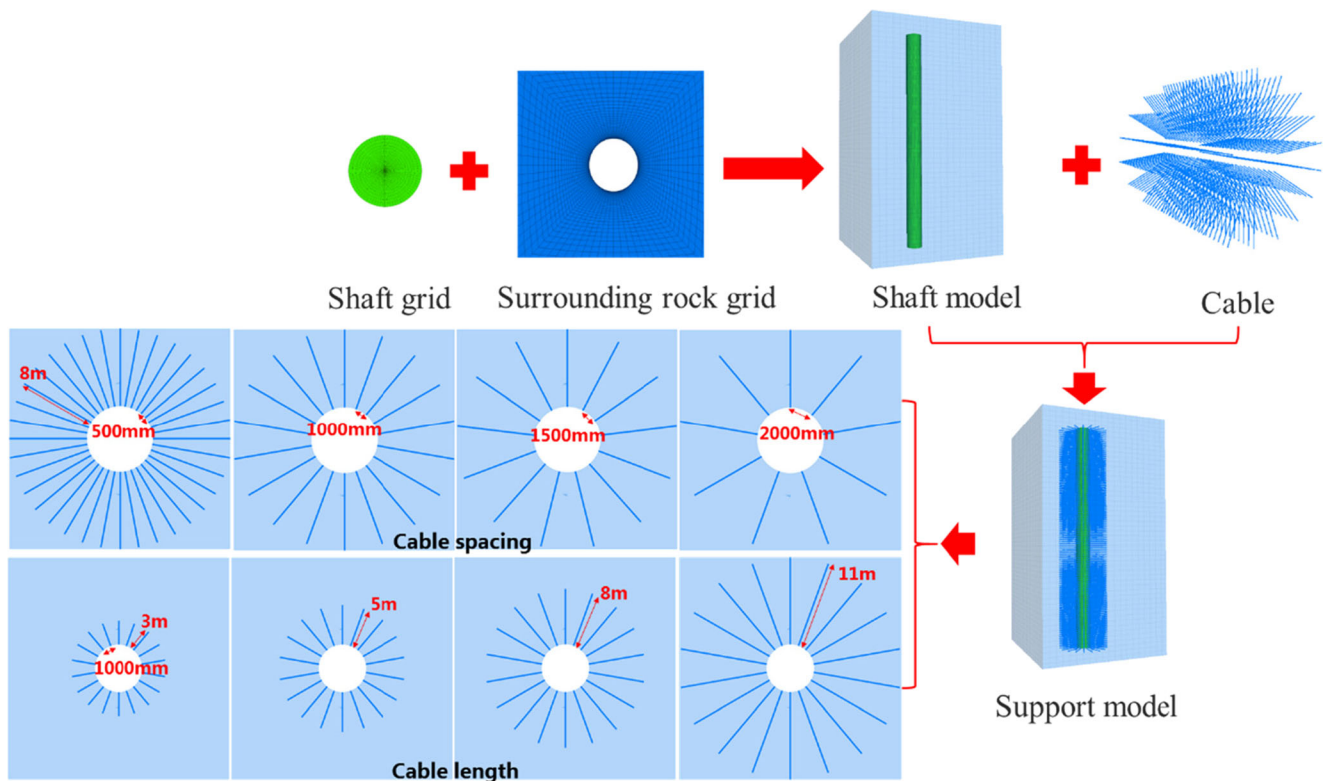


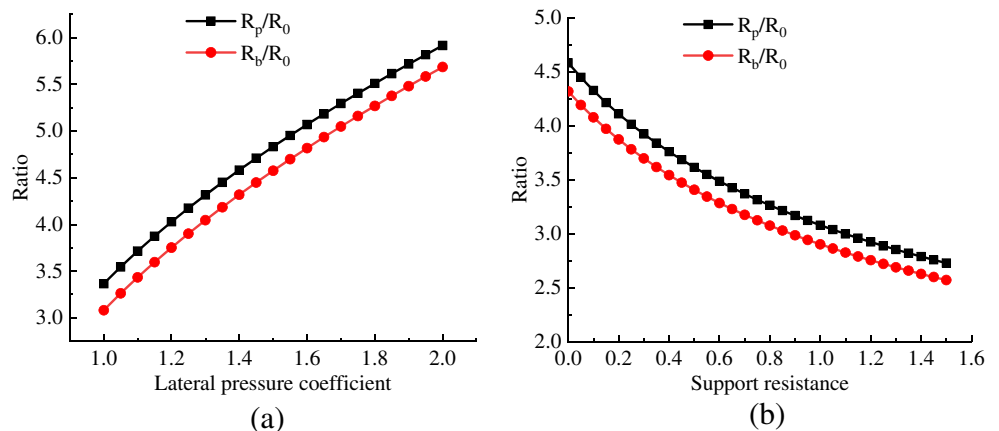
Fig. 8 The optimization process of NPR cable support

shear plastic volume,  $V$  is the total volume) to represent the shear failure characteristics of the shaft surrounding rock, and the tensile failure (tensile failure is defined as  $D_t = \frac{V_t}{V} \times 100\%$ , where  $V_t$  is the total tensile plastic volume,  $V$  is the total volume) to represent the tensile failure characteristics of the shaft surrounding rock. Shear failure, rather than tensile failure, is the primary failure under no support scheme. The shear damage increased linearly as the NSF coefficient increased. The shear failure ranged from 8.4 to 29.35%, as the NSF coefficient increased from 1 to 2. In the whole process, the changes of tensile failure were not obvious.

### Optimization of NPR cable spacing

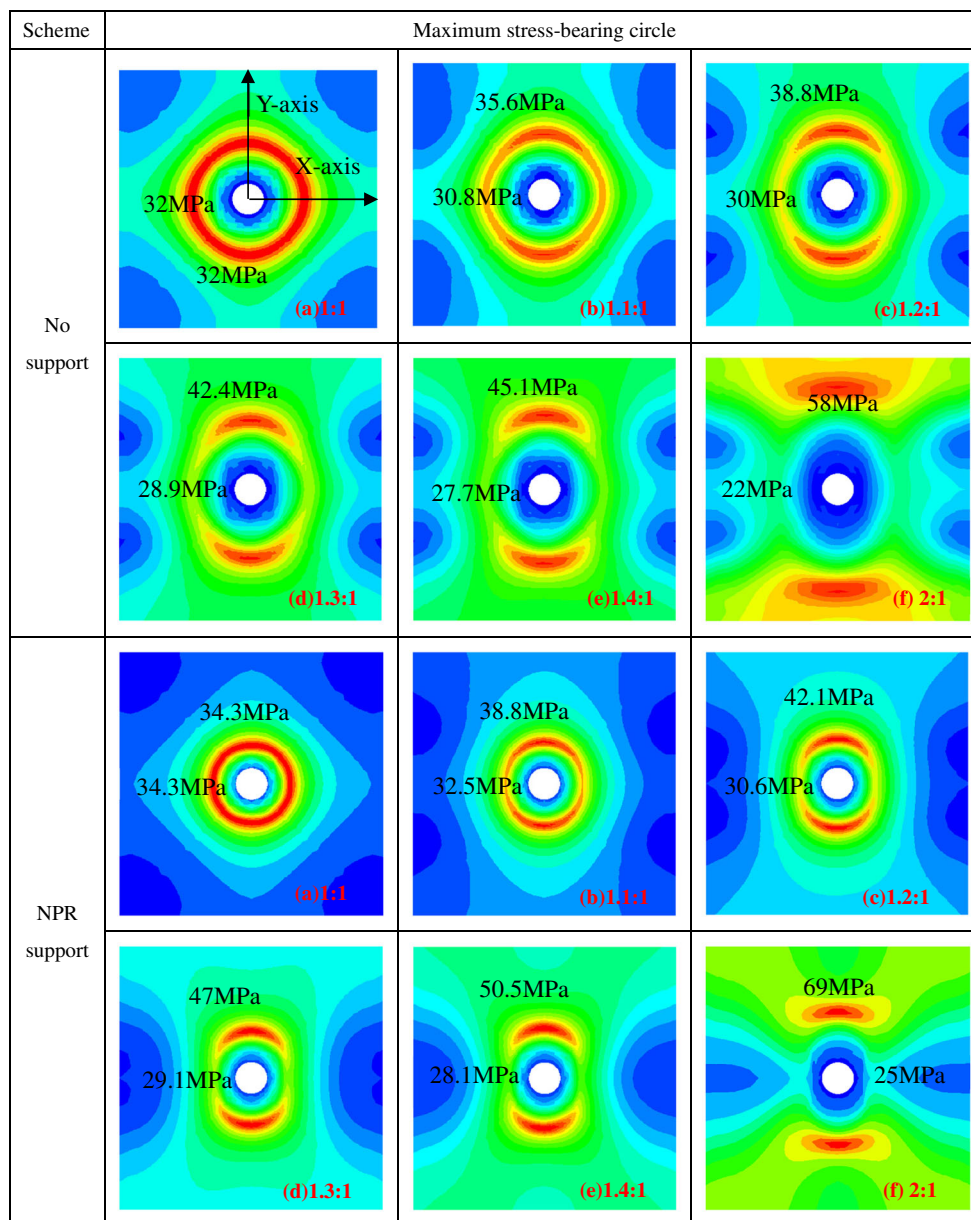
Figure 14 shows the distribution characteristics of the maximum stress-bearing circle and plastic zone with different support spacing. The results showed that the maximum stress-bearing circle expanded to the depth of the surrounding rock as the support space increased. The peak stress decreased with the increase of spacing in the  $y$ -axis direction. The maximum stress in the  $y$ -axis direction ranged from 51.7 to 48.4 MPa as space increased from 500 to 2000 mm. The peak stress in the  $x$ -axis also decreased as the increased spacing, as shown in Fig. 13. The maximum stress in the  $x$ -axis direction ranged

Fig. 9 Change curves of the maximum plastic zone and broken zone under different lateral pressure coefficient and support resistance: **a** lateral pressure coefficient; **b** support resistance





**Fig. 10** The maximum stress-bearing circle under no support and NPR support scheme



from 29 to 27.8 MPa as spacing increased from 500 to 2000 mm.

Figure 15 shows the stress curves and radius ratio under different spaces. As spacing increased from 500 to 2000 mm, the radius ratio in the y-axis direction increased from 3.73 to 4.8 (Fig. 15b), and the radius ratio in the x-axis direction increased from 2.547 to 3.43 (Fig. 15b). It indicated that the bearing structure of the surrounding rock was far from the shaft as the spacing increased.

The plastic zone of the shaft surrounding rock presents the elliptical shape (Fig. 14). Figure 13 shows the failure characteristics of the shaft surrounding rock under different support spacing. The whole process is dominated by shear failure with less tensile failure. The bigger the cable spacing was, the more obvious the shear failure was. The tensile failure was not

obvious. When the support spacing was 500 mm, the shear failure was 4.6%, while shear failure was 8.3% with the space of 2000 mm.

$$P = \frac{V_{shear} + V_{tension}}{V_0} \tag{8}$$

$$B = P_1 - P \tag{9}$$

To show the support effect of constant resistance cable, we use the support failure and support compensation for comparative analysis (Fig. 16), where  $P$  is the support failure, %;  $V_{shear}$  is the volume of support shear failure,  $m^3$ ;  $V_{tension}$  is the volume of support tension failure,  $m^3$ ;  $V_0$  is the total volume,  $m^3$ ;  $P_1$  is the unsupported failure,  $m^3$ ;  $B$  is the support

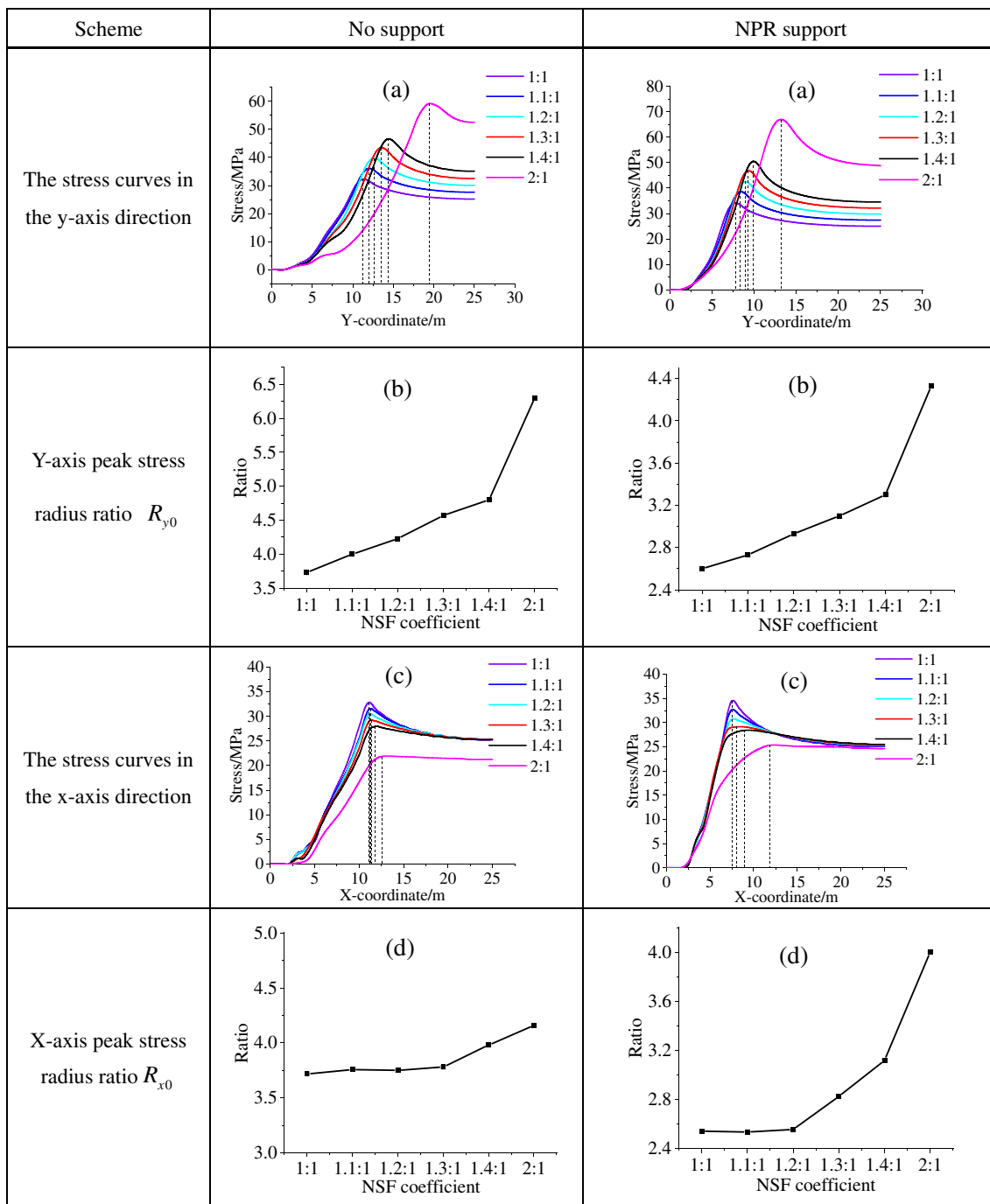


**Fig. 11** The stress and radius ratio under no support and NPR support: (a) the stress curves in the y-axis direction; (b) Y-axis peak stress radius ratio  $R_{y0}$ ; (c) the stress curves in the x-axis direction; (d) X-axis peak stress radius ratio  $R_{x0}$

compensation, %. The total volume of the model  $V_0$  is obtained by using fish language in FLAC3D. Similarly, the volume of support shear failure  $V_{shear}$  and tensile failure  $V_{tension}$  are obtained from the model by fish language in FLAC3D.

With the increase of support spacing, the support failure increased, while the support compensation decreased. The support played an important role and prevented the shallow surrounding rock from extending to a large failure. For the support

scheme with a space of 500 mm, the support failure and compensation were 36.2% and 63.7%, respectively. When the support spacing increased to 2000 mm, the support failure increased to 65.4%, and the compensation decreased to 34.5%.

It can be concluded that the support scheme with the support spacing of 500mm was the best support spacing, but the number of cables was increased by 100% compared with the space of 1000mm. As the cable spacing ranged from 500 to

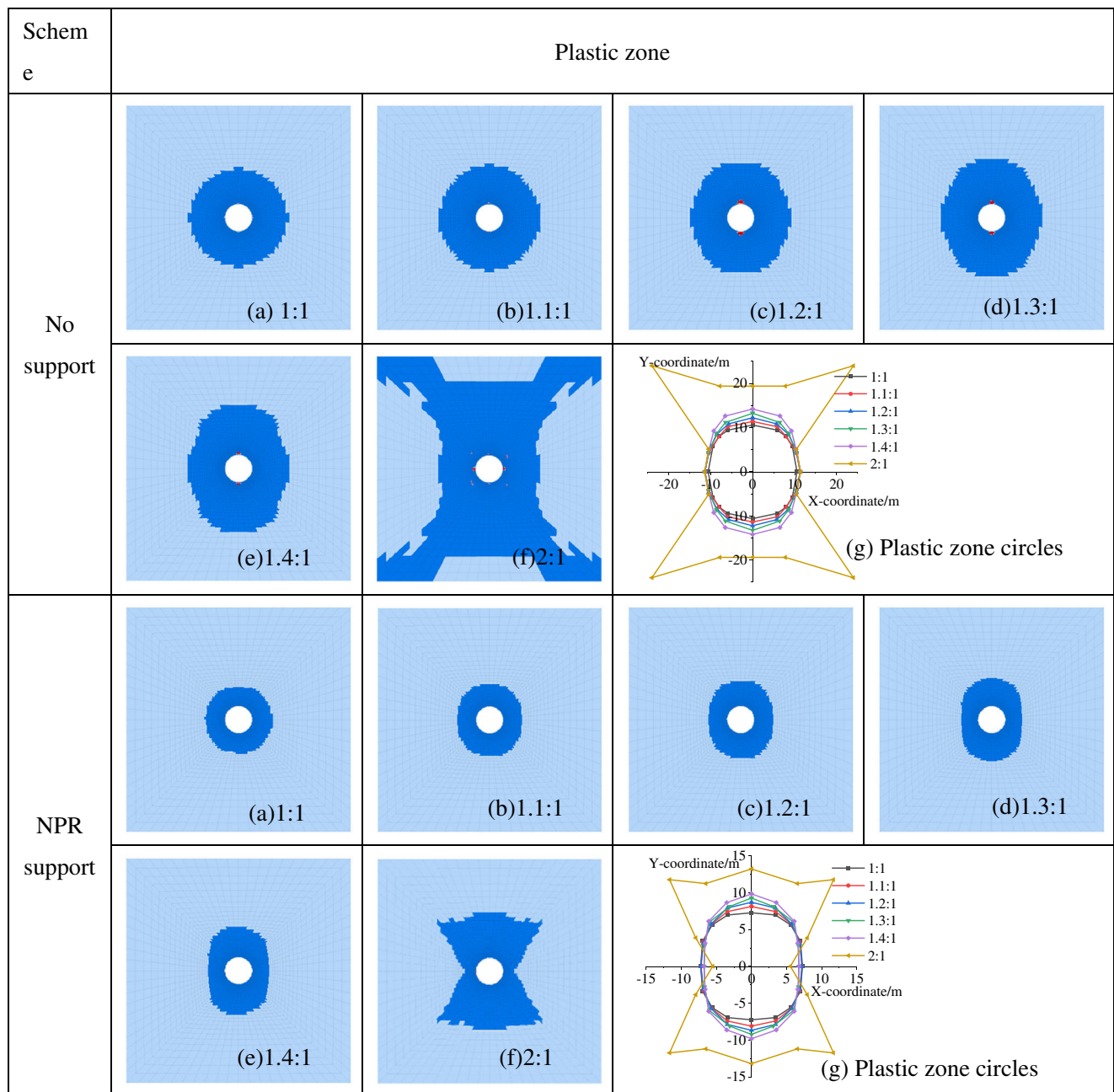


Fig. 12 Distribution characteristics of maximum plastic zone under no support and NPR support scheme

1000 mm, the support failure increased from 36.28 to 48.16%, increased by 24.66%. The support compensation has decreased from 63.71 to 51.83%, decreased by 22.92%. The shear failure increased from 4.6 to 6.1% and increased by 24.5%. In general, the number of cables had reduced by half, but the support effect was better. Therefore, the scheme with a space of 1000 mm is selected as the better support scheme.

**Optimization of NPR cable length**

The cable space of 1000 mm was selected as a better scheme. The plastic zone was in a small range. The stress-bearing

circle was close to the shaft. Four schemes with the cable length of 3m, 5m, 8m, and 11m were analyzed under the cable space of 1000 mm.

Figure 17 shows the distribution characteristics of the maximum stress-bearing circle and plastic zone of the surrounding rock under different cable lengths. Four schemes with cable lengths of 3m, 5m, 8m, and 11m are selected for comparative analysis. According to the distribution characteristics of the maximum stress-bearing circle, the range of maximum stress-bearing circles decreased as the increase of cable length, while the peak stress in the y-axis direction increased. The peak stress in the y-axis direction increased from 46.8 to 48.2MPa

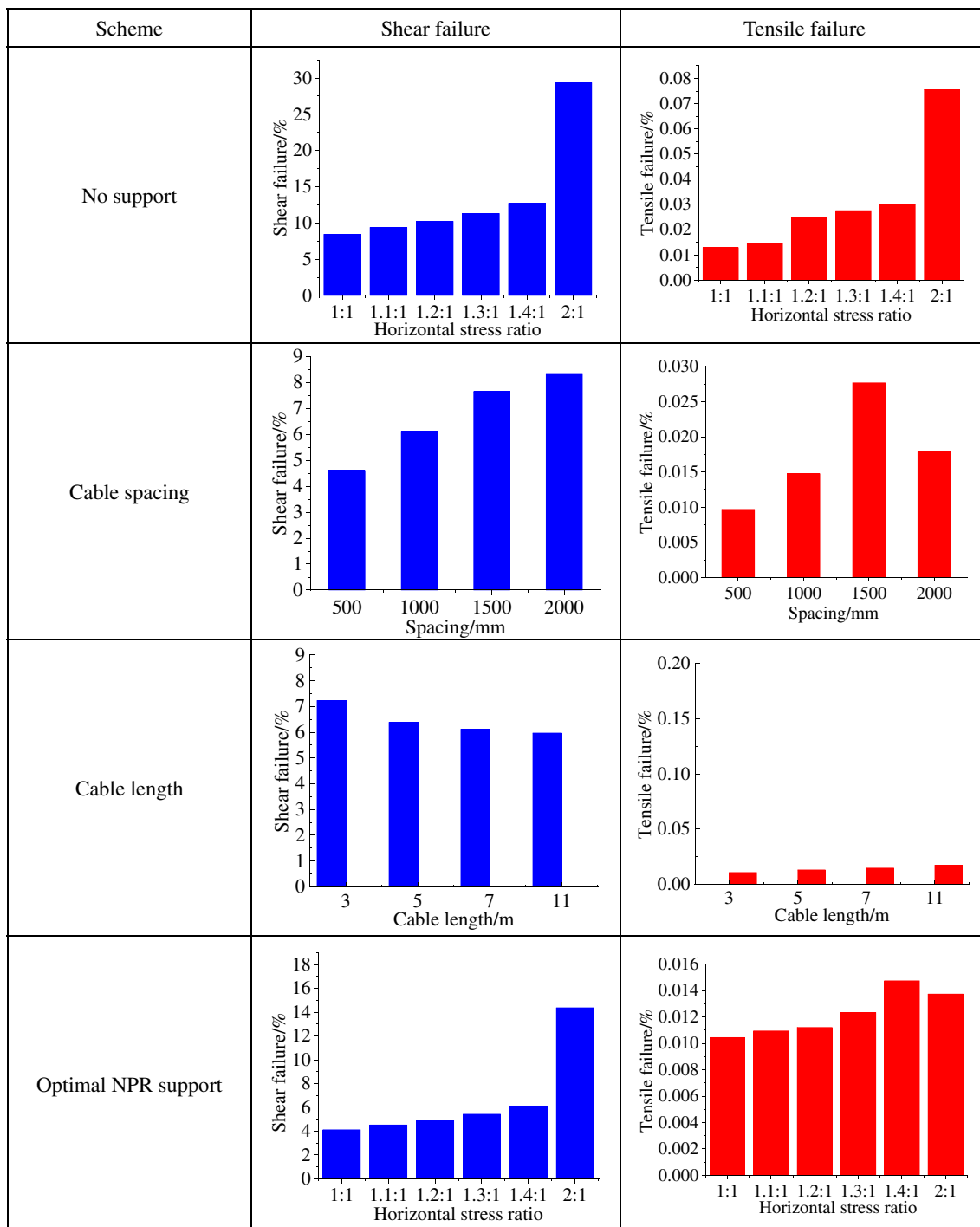


Fig. 13 Failure characteristics of the plastic zone under no support, different cable spacing, different cable length and NPR support scheme

as the cable length increased from 3 to 11 m. The change of peak stress in the *x*-axis direction is not obvious, as shown in Fig. 17.

Figure 18 shows the stress curves and radius ratio under different cable lengths. As the cable length increased from 3 to 11 m, the radius ratio in the *y*-axis direction decreased from 4.3 to 3.7, and the radius ratio in the *x*-axis direction decreased from 3.47 to 3.15, which indicated that the bearing structure of

the surrounding rock was close to the shaft as the cable length increased (Fig. 18b).

Figure 13 shows the failure characteristics of the surrounding rock of the shaft under the support conditions of different cable lengths. The shear failure was the main failure pattern. The failure of shaft decreased as the increase of cable length. When the cable length is 3 m, the shear failure of the surrounding rock was the least, in which the value was 7.2%. When the

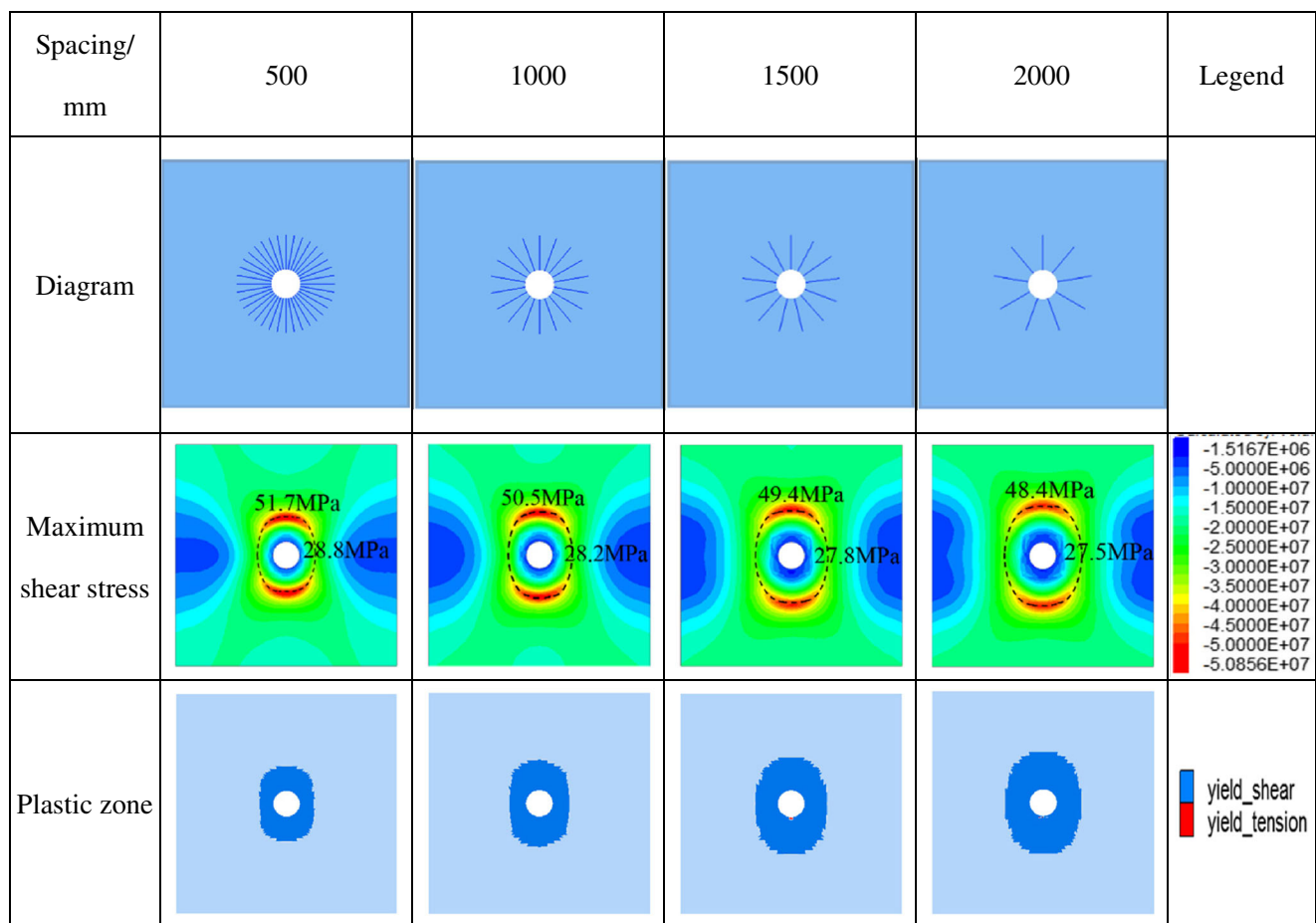


Fig. 14 Distribution characteristics of maximum stress-bearing circles and plastic zone in different support schemes

support length increased to 11 m, the shear failure of the shaft surrounding rock decreased to 5.9%, and the tensile failure is very small in the whole process.

It can be seen from Fig. 19 that the support failure decreased obviously as the cable length increased, while the support compensation increased. The support failure curve showed a trend of slowing down, and the support compensation curve showed a trend of slowing growth. The support failure reduced by 4.36%, and support compensation increased by 4.05% as the cable length increased from 5 to 8 m. The support failure reduced by 2.34%, and support compensation increased by 2.07% as the cable length increased from 8 to 11 m. When the cable length was 8 and 11 m, the support compensation was more than 50%. Comprehensive consideration showed that it was more cost-effective to select cable length of 8 m.

**Stress and plastic zone distribution under NPR cable**

The optimal support scheme with the cable space of 1000 mm and the cable length of 8 m was selected to apply to control the stability of shaft in the NSF. Figure 10 shows the maximum

stress-bearing circles of the shaft surrounding rock under the optimal support scheme.

As the NSF coefficient increased, the maximum stress in the *y*-axis direction increased, and the stress in the *y*-axis direction decreased, as shown in Fig. 10. The peak value of stress in the *y*-axis direction increased from 32 MPa, 35.6 MPa, 38.8 MPa, 42.4 MPa, 45.1 MPa, and 58 MPa under no support to 34.3 MPa, 38.8 MPa, 42.1 MPa, 47 MPa, 50.5 MPa, and 69 MPa under NPR cable support, which increased by 7.18%, 8.99%, 8.5%, 10.85%, 11.97%, and 18.9%, respectively. The stress in the *x*-axis direction also improved compared with no support scheme. Figure 11 shows the distribution characteristics of stress curves and radius ratio in the *y*-axis direction after NPR cable support. The radius ratio in the *y*-axis direction was in the range of 3.73 to 6.3 under no support, while the radius ratio was reduced to the range of 2.5 to 4.3 after NPR cable support. The radius ratio in the *x*-axis direction was in the range of 3.73 to 4.1 under no support, while the radius ratio was reduced to the range of 2.5 to 4.0 after NPR cable support. The results showed that NPR cable support could effectively improve the stress state of near-field surrounding rock and increase the bearing capacity of the surrounding rock.

**Fig. 15** The stress and radius ratio under different spaces: **a** the stress curves in the  $y$ -axis direction; **b**  $Y$ -axis peak stress radius ratio  $R_{y0}$ ; **c** the stress curves in the  $x$ -axis direction; **d**  $X$ -axis peak stress radius ratio  $R_{x0}$

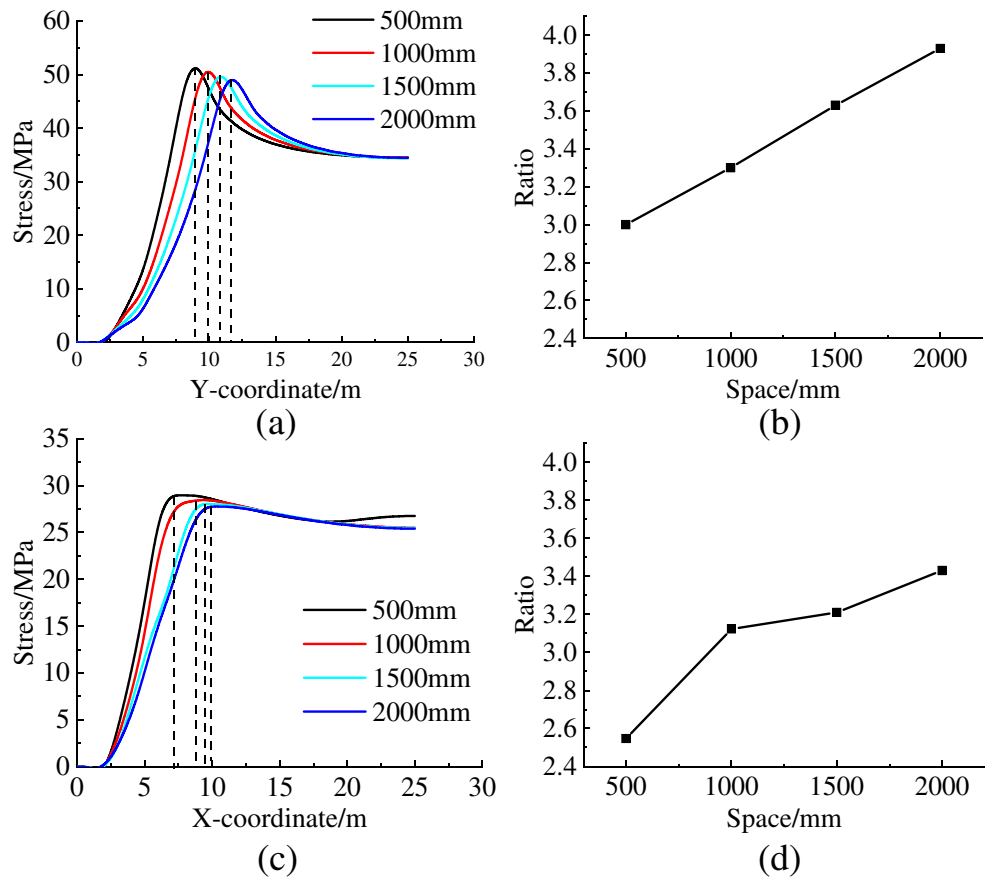
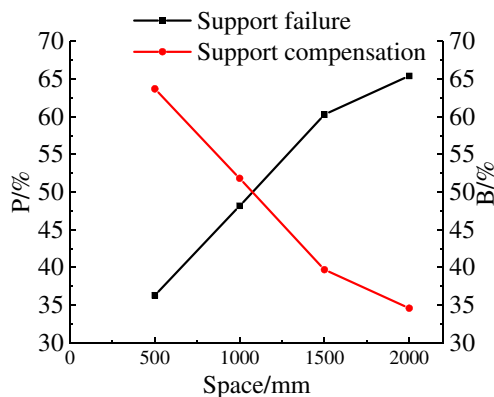


Figure 12 shows the extension range of the plastic zone under NPR cable support. The plastic zone of the surrounding rock of the shaft presented the elliptical shape with the long axis in the  $y$ -axis direction. As the NSF coefficient increased, the elliptical effect of the plastic zone was more obvious. Compared with no support, the radius of the plastic zone in the  $y$ -axis direction was reduced from 10~19.4 to 7~13 m after NPR cable support. The radius of the plastic zone in the  $x$ -axis direction was stable in the range of 5~8m. The NPR cable support significantly reduced the expansion range of the plastic zone of the surrounding rock.



**Fig. 16** Support and compensation curves of different support schemes

Figure 13 shows the failure characteristics under NPR cable support. Figure 20 shows the reduction of failure after NPR support.  $K = (f_N - f_S)/f_N$ , where  $f_N$  is the failure under no support, and  $f_S$  is the failure under NPR support.  $K$  is the reduction of failure. Compared with no support, the shear and tensile failure of the surrounding rock significantly reduced (Fig. 13 and Fig. 20). The shear failure of the shaft under no support was 8.4%, 9.3%, 10.2%, 11.3%, 12.6%, and 29.35%, respectively. The shear failure of the shaft after support was 4.1%, 4.5%, 4.9%, 5.4%, 6.1%, and 14.38%, reducing by 51.2%, 51.6%, 51.9%, 52.2%, 51.5%, and 51% (Fig. 20). The reduction of shear failure was more than 50% after NPR support. What's more, the reduction of tensile failure also increased, especially when the coefficient of NSF was 1.2, 1.3, 1.4, and 2, the reduction was more than 55%. Therefore, the new support scheme could effectively control the failure of the shaft in the NSF.

### Field analysis

According to the measured in situ stress data of Daqiang coal mine, the maximum principal stress and the minimum principal stress were in the north-south and east-west directions of the shaft, respectively. A surface displacement observation station was set up near the shaft of ingate, as shown in Fig.

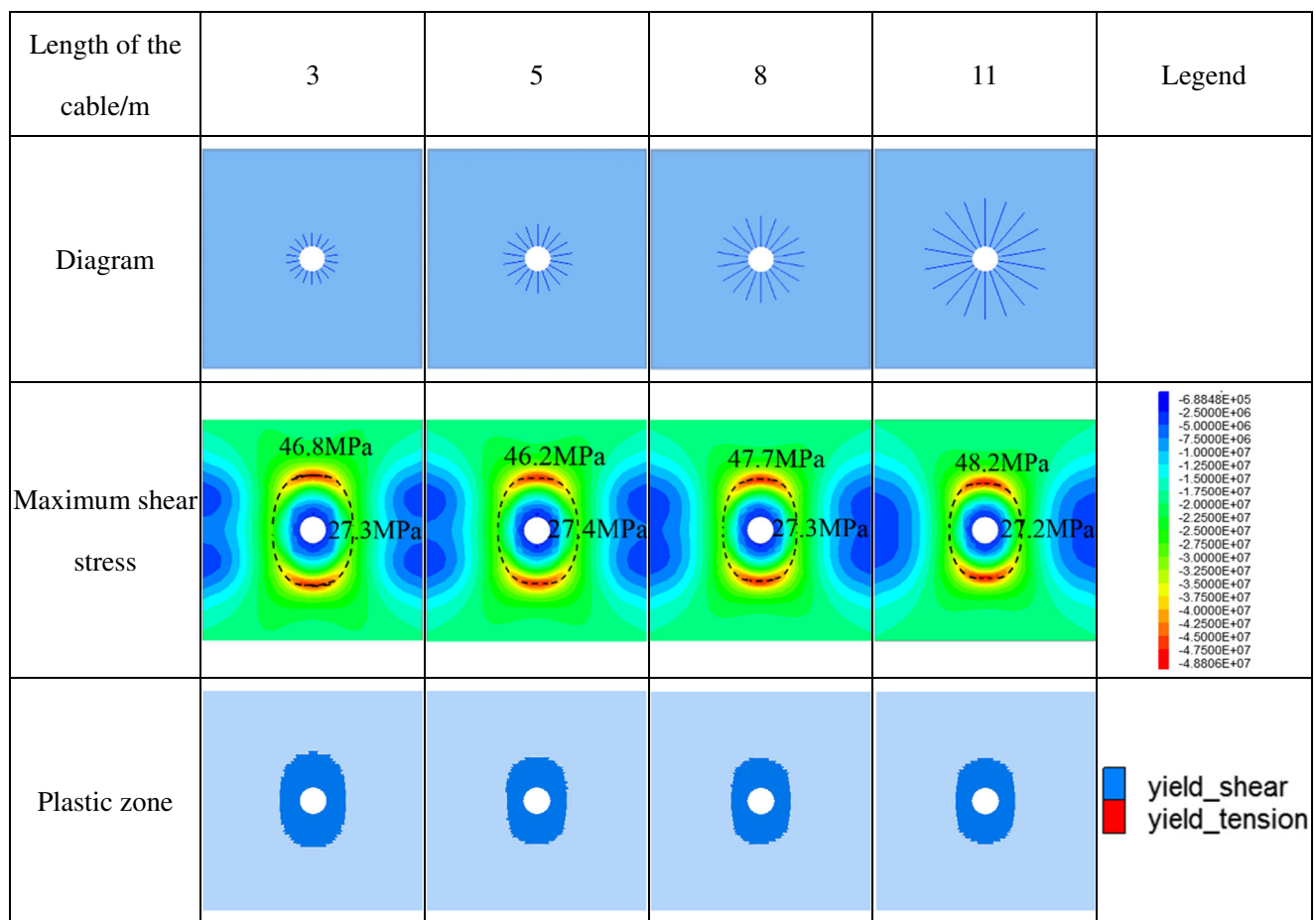


Fig. 17 Distribution characteristics of stress-bearing circles and plastic zone with different cable lengths

2. Figure 21 shows the shaft deformation curves in filed test. Surface displacement had been observed for more than 6 months. The deformation started to be stable around 30 days after support. However, the shaft was affected by two times of excavation of the roadway, and the deformation increased twice, but the increment was small. The maximum shrinkage deformation of the shaft was 88mm, and the shaft was less affected by excavation.

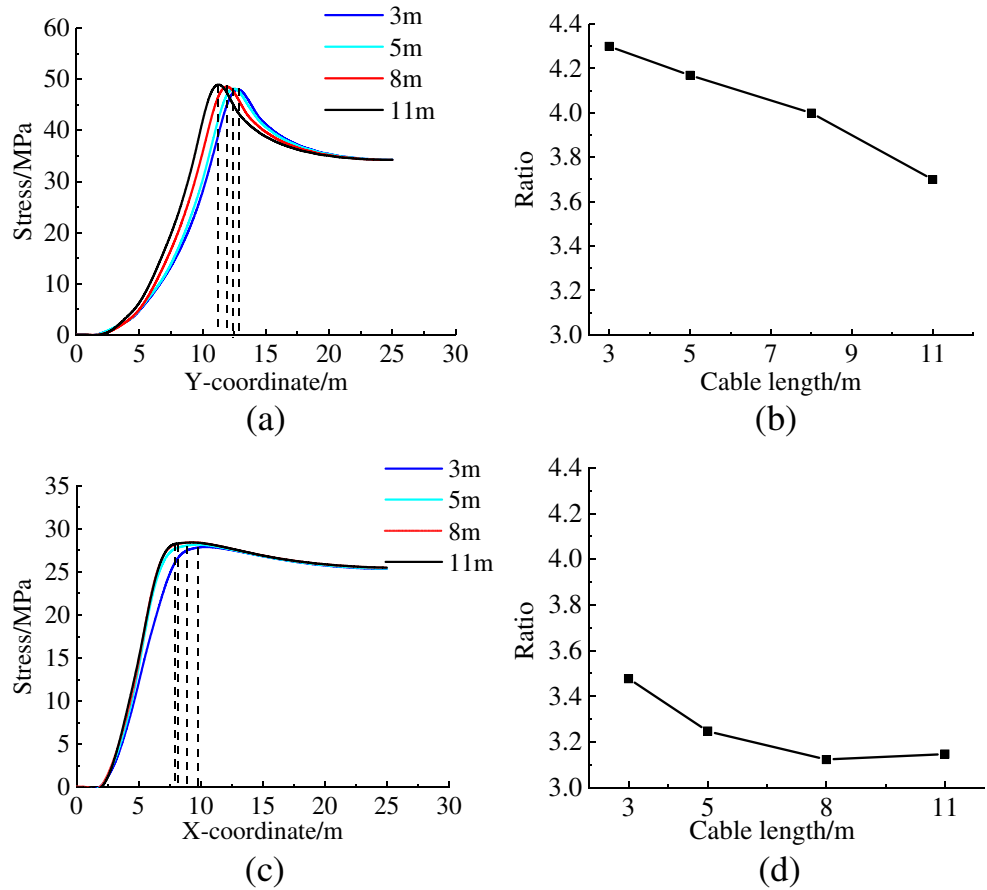
Figure 22 shows the shaft deformation curves in numerical simulation test. In the numerical model, the direction of *x*-axis is the direction of maximum horizontal principal stress, and the direction of *y*-axis is the direction of minimum horizontal principal stress. Similar to the field results, the maximum deformation occurs in the direction of the minimum principal stress. Because the stress in the direction of the maximum principal stress is transferred to the direction of the minimum principal stress, the surrounding rock in the direction of the minimum principal stress is seriously damaged. In numerical simulation test, the maximum deformation is 93 mm and minimum deformation is 45 mm. However, the maximum deformation is 88 mm and minimum deformation is 63 mm in field test. There is little deformation gap between the numerical simulation test and the field test, which indicated that NPR

cable support and flexible support could ensure the stability of the shaft and meet the deformation requirements of the shaft under the condition of NSF.

### Discussion

Shaft failure usually comes from the interaction between the shaft surrounding rock and the shaft wall. The failure of shaft wall is usually caused by local shear and tensile failure. When the contact between the surrounding rock and the shaft wall is not uniform, the shaft wall will be damaged. The non-uniform stress of shaft surrounding rock usually comes from the inhomogeneous lithology (Sun et al. 2018), structure (Gough and Bell 1982), in situ stress (Guo et al. 2008), and seepage (Li et al. 2018) of the surrounding rock. This paper mainly focused on the failure of the shaft surrounding rock caused by the non-uniform stress field. In the model, when the NSF is 1, the failure and stress distribution of the surrounding rock are uniform. Of course, this is a very ideal state, which almost does not exist in deep shaft surrounding rock. There are more non-uniform stress fields in deep surrounding rock. He (2021) showed the non-uniform pressure of the surrounding rock at

**Fig. 18** The stress and radius ratio under different cable length: **a** the stress curves in the  $y$ -axis direction; **b**  $Y$ -axis peak stress radius ratio  $R_{y0}$ ; **c** the stress curves in the  $x$ -axis direction; **d**  $X$ -axis peak stress radius ratio  $R_{x0}$



different depths by measurement. Li et al. (2012) also shows that the non-uniform stress field coefficient of China's in situ stress level for 1000m is 0.5~2.5. However, with the increase of mining scope and intensity of coal mine, the shaft construction is developing towards the direction of deep mining. Therefore, it is significant to study the stress and failure characteristics of deep shaft surrounding rock.

In order to avoid the non-uniform pressure action of shaft surrounding rock and shaft wall under the non-uniform stress field, the surrounding rock of shaft needs effective primary

support. Aiming at the deep non-uniform stress field of the shaft, He (2021) proposed two models for deep shaft construction, including the use of NPR cable for primary support in deep shaft. He also pointed out that the constant resistance of the current NPR cable could reach 500 kN, and the deformation of the cable can reach 1m, which could effectively control the large deformation of deep shaft surrounding rock. What's more, the NPR anchor cable has the characteristic of constant resistance. Under the support of the NPR cable, the shaft surrounding rock pressure after deformation is uniform, which is

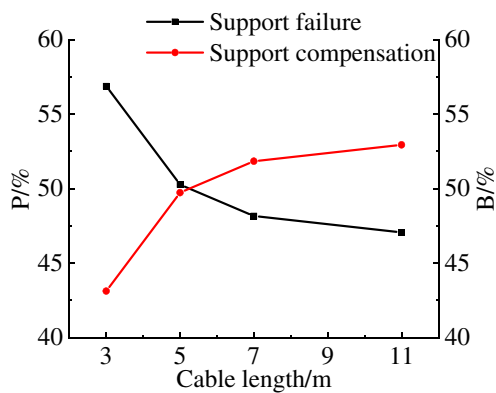


**Fig. 19** Support and compensation curves of the plastic zone with different cable lengths

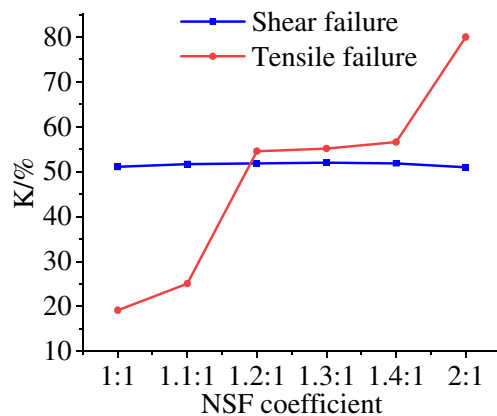


**Fig. 20** The reduction of damage after NPR support



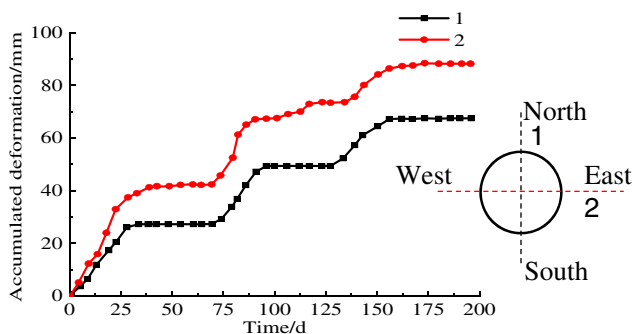


Fig. 21 Shaft deformation curves in field test

equal to the constant resistance value. Therefore, NPR cable can effectively control the deformation caused by non-uniform stress. For deep shaft support, it may be an effective way to adopt NPR constant resistance support for the primary support and shaft lining support for the secondary support.

### Conclusion

In this paper, a plane strain model and a numerical simulation model were established to analyze the stress, plastic zone, and control characteristics of the shaft surrounding rocks under non-uniform stress field. First, the characteristics of maximum stress-bearing circle and plastic zone were analyzed under no support. Then, based on NPR cable, the optimal control process of the surrounding rock is proposed. Finally, the optimal scheme is successfully applied to control shaft surrounding rock in numerical simulation and field test. The detailed conclusions are as follows:

1. According to the theoretical analysis, the maximum stress-bearing circle and plastic zone were greatly influenced by the NSF factor and support resistance. As the NSF coefficient increased, the radius of

maximum stress-bearing circle and the radius of the plastic zone was far from the shaft, which indicated that the shallow surrounding rock suffered from severe failure. However, the radius of the maximum stress-bearing circle and the radius of the plastic zone were close to the shaft with the increase of support resistance. The support resistance improved the bearing capacity.

2. A numerical model was established to analyze the maximum stress-bearing circles and plastic zone by considering six NSF coefficients. The maximum stress-bearing circle and plastic zone increased with the increase of the NSF coefficient. Due to the transfer and superposition of stress to  $y$ -axis, the peak stress in the  $y$ -axis direction increased, while the peak stress in the  $x$ -axis direction decreased. However, the change of the plastic zone in the  $x$ -axis was not obvious.
3. To get a better support scheme, the cable support schemes with four cable spaces and four cable lengths were put forward to select the optimal support scheme. The optimal support scheme with cable space of 1000 mm and cable length of 8 m was obtained by comparing characteristics of the maximum stress-bearing circle, plastic zone, shaft failure, and support compensation curves. The numerical results indicated that the optimal support scheme reduced the plastic zone and failure significantly, which effectively improved the bearing capacity of the surrounding rock of shaft.
4. The NPR cable support scheme was applied in the field test. The maximum deformation is 88 mm in field test and 93 mm in numerical simulation test. There is little deformation gap between the numerical simulation test and the field test. The results showed that NPR cable support could meet the requirements of the shaft, which provided guidance for shaft support.

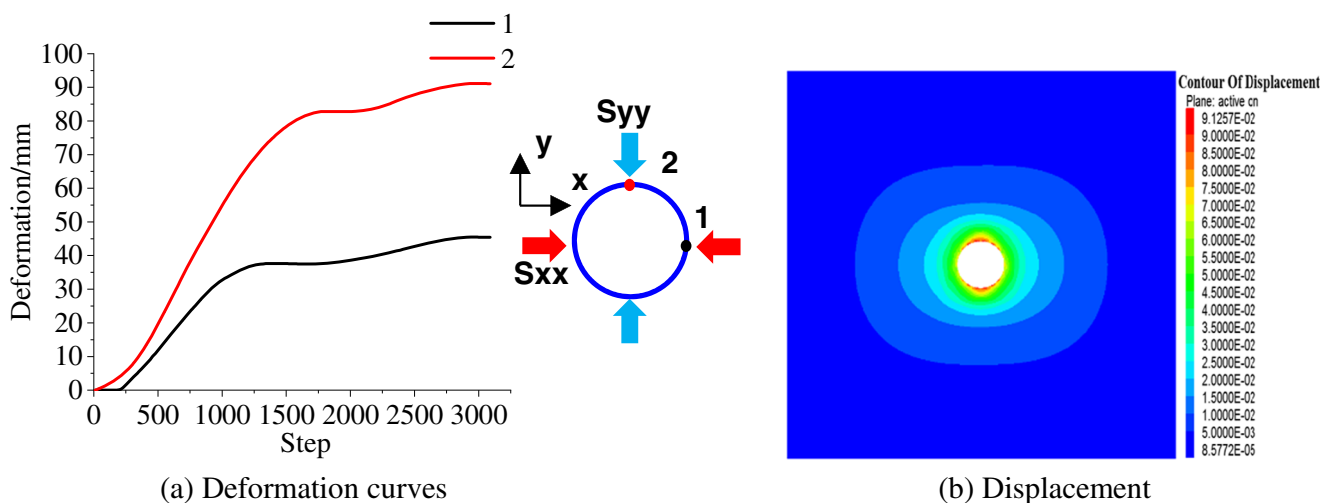


Fig. 22 Shaft deformation curves in numerical simulation test. a Deformation curves. b Displacement

5. There is still a lot of research to be done on the cable support problem. In the future, we will continue to study non-uniform cable support.

**Funding** This work was supported by the National Key Research and Development Plan of China (Grant No. 2016YFC0600901), the National Natural Science Foundation of China (Grant No. 51874311), the Natural Science Foundation of China (Grant No. 51904306), and the Special Fund of Basic Research and Operating of China University of Mining and Technology, Beijing (Grant No. 2009QL03)

**Data availability** The data used to support the findings of this study are available from the corresponding author upon request.

## Declarations

**Conflict of interest** The authors declare that they have no competing interests.

## References

- Akl SA, Whittle AJ (2016) Validation of soil models for wellbore stability in ductile formations using laboratory TWC tests. *J Geotech Geoenviron Eng* 143(2):04016095
- Cheng H, Cai HB, Rong CC, Yao ZS, Li MJ (2011) Rock stability analysis and support countermeasure of chamber group connected with deep shaft. *J China Coal Soc* 36(02):261–266
- Ge XG (2002) Engineering properties of two grouting techniques in mending shaft-lining ruptures. *J China Coal Soc* 27(1):41–44
- Gough DI, Bell JS (1982) Stress orientations from borehole wall fractures with examples from Colorado, East Texas, and Northern Canada. *Can J Earth Sci* 19(7):1358–1370
- Guo L, Qi S, Yang C (2008) Analysis on uneven side pressure affected to mine shaft stressed. *Coal Eng* 11:65–68
- He MC (2021) Research progress of deep shaft construction mechanics. *J China Coal Soc* 46(03):726–746
- He MC, Gong WL, Wang J, Qi P, Tao ZG, Du S, Peng YY (2014a) Development of a novel energy-absorbing bolt with extraordinarily large elongation and constant resistance. *Int J Rock Mech Min Sci* 67:29–42
- He MC, Wang J, Sun XM, Yang XJ (2014b) Mechanics characteristics and applications of prevention and control rock bursts of the negative poisson's ratio effect anchor. *J China Coal Soc* 39(2):214–221
- He MC, Li C, Gong WL (2015) Elongation and impacting experimental system for bolts with constant resistance and large deformation and finite element analysis. *Chin J Rock Mech Eng* 24(11):2179–2187
- He MC, Li C, Gong W, Wang J, Tao, ZG (2016) Support principles of NPR bolts/cables and control techniques of large deformation. *Chin J Rock Mech Eng* 35(8):1513–1529
- Kang HP, Lin J, Yang JH, Wu YZ, Gao FQ (2010) Study and practice on combined technology for reinforcing soft and fractured shaft. *J Min Safety Eng* 27(04):447–452
- Li XP, Wang B, Zhou GL (2012) Research on distribution rule of geostress in deep stratum in Chinese mainland. *Chin J Rock Mech Eng* 31(S1):2875–2880
- Li XR, Jaffal H, Feng YC, Mohtar CE, Gray KE (2018) Wellbore breakouts: Mohr-Coulomb plastic rock deformation, fluid seepage, and time-dependent mudcake buildup. *J Nat Gas Sci Eng* 52:515–528
- Pan Y, Zhao GM, Meng XR (2015) Elasto-plastic analysis on surrounding rock mass under non-uniform stress field. *J China Coal Soc* 36(S1):53–57
- Strickland B, Board M, Sturgis G, Berberick D (2016) Elliptical shaft excavation in response to depth induced ground pressure. *Proceedings of the SME Annual Meeting*. Phoenix, Arizona, In
- Sun XM, Wang D, Wang C, Liu X, Zhang B, Liu ZQ (2014) Tensile properties and application of constant resistance and large deformation bolts. *Chin J Rock Mech Eng* 33(9):1765–1771
- Sun XM, Li G, Zhao CW, Liu YY (2018) Investigation of deep mine shaft stability in alternating hard and soft rock strata using three-dimensional numerical modeling. *Processes* 7(1):1–2
- Walton G, Kim E, Sinha S, Sturgis G, Berberick D (2018) Investigation of shaft stability and anisotropic deformation in a deep shaft in Idaho, United States. *Int J Rock Mech Min Sci* 105:160–171
- Wang WM (1993) Stress analysis of shaftwall 1000 m deep and problems in design. *J China Coal Soc* 18(005):63–72
- Xu HD, Jing LW, Yang RS (2005) Analysis of shear force between surface soil and vertical shaft in mine. *Chin J Rock Mech Eng* 25(02):385–391
- Yan H, Zhang JX, Zhou N, Zhang S, Dong XJ (2018) Shaft failure characteristics and the control effects of backfill body compression ratio at ultra-contiguous coal seams mining. *Environ Earth Sci* 77(12):458.1–458.12
- Yang XJ, Pang JW, Zhang BT, Meng FY, Jiang WF, Fan LP, Niu X (2014) Deformation and failure mechanism and support measures of the soft rock roadway in the air return laneway. *J China Coal Soc* 39(06):1000–1008
- Yao ZS, Cheng H, Rong CX (2010) Shaft structural design and optimization of deep freezing bedrock shaft in west area. *J China Coal Soc* 35(5):760–764
- Yao ZS, Song HQ, Cheng H, Rong CX (2012) The experimental study on inner shift lining structure of freezing shaft in deep thick aquiferous soft rock. *Life Sci* 4(19):1839–1841
- Zhang Y, Sun XM, Zheng YL, Li JB, Guo ZB, Zhang B (2019) An anti-punching and energy-releasing coupling support technology in deep mining roadway and its application. *Chin J Rock Mech Eng* 38(9):1860–1869